Extending the Spherical Planetary Radiation Pressure Acceleration Model to Optical Solar Sails

Carzana, L.; Visser, P.N.A.M.; Heiligers, M.J.

DOI
10.2514/1.G008940

Publication date
2025

Document Version
Final published version

Published in
Journal of Guidance, Control, and Dynamics: devoted to the technology of dynamics and control

Technical Notes

Extending the Spherical Planetary Radiation Pressure Acceleration Model to Optical Solar Sails

Livio Carzana,* Pieter Visser,† and Jeannette Heiligers‡
Delft University of Technology, 2329 HS Delft, The Netherlands

https://doi.org/10.2514/1.G008940

I. Introduction

SOLAR sailing is a propulsion method that makes use of solar radiation pressure (SRP) as the primary source of thrust [1]. Due to its propellantless nature, solar sailing has drawn increasing attention in the scientific community in recent years, with several studies investigating its use particularly for heliocentric science missions and future space exploration [2,3]. Although there is potential for such applications, most solar sails flown to date have only been used as technology demonstrators, from JAXA's IKAROS sailcraft [4] (the first to successfully demonstrate the technology), to the recently launched Advanced Composite Solar Sail System (ACS3) by NASA [5]. The vast majority of these demonstrators have flown around the Earth. As the technology matures, near-future solar-sail missions are also expected to remain Earth-bound to further explore the feasibility of solar sailing for different applications [6,7], such as in-orbit servicing and active debris removal [8–10]. In addition to gravity and SRP, the solar-sail dynamics are affected by several sources of perturbations in proximity of the Earth, including eclipses, atmospheric drag [11–13], and notably, planetary radiation pressure (PRP) [14–16]. The PRP acceleration and its effect on the solar-sail dynamics and control have been investigated only to a first-order extent. Preliminary studies have shown that PRP acceleration can reach magnitudes of 20% of the SRP acceleration around the Earth [16]. Such a large perturbation warrants for the accurate modeling of the PRP acceleration, both for sail calibration [17] and detailed mission design of future near-Earth missions. In these studies, the Earth planetary radiation is modeled using analytical models, specifically the finite-disk radiation model by McInnes [14,15] and the so-called "spherical sinusoidal" radiation model developed by Carzana et al. [16], which accounts for the spherical shape of the Earth and its varying brightness depending on the sail's altitude and location. However, both these models assume the sail to be ideal (i.e., perfectly reflecting), which introduces an approximation that limits the fidelity of the solar-sail dynamics. In addition to these analytical models, numerical models exist that allow for a higher fidelity [18–23], particularly in the way they model the geographical distribution of planetary radiation flux. This is done by representing the surface of the Earth as a set of facets, each with known radiation flux and its variation over time. The limitation of numerical models, however, is the significantly high computational cost they require, especially compared to analytical models, which can be more than 30 times computationally faster [16]. Furthermore, the numerical nature of these models can also pose limitations when using routines that require analytical knowledge of the PRP acceleration's derivatives. Among these, for example, are several (gradient-based) trajectory optimization algorithms [24], as well as precise orbit determination and estimation routines [25]. In light of the aforementioned, the need for an analytical model that can efficiently, yet accurately, determine the PRP acceleration arises. Such a model could be effectively used to perform detailed orbit analysis for Earth-bound (or planetocentric) solar-sail missions. The model would also enable the accurate optimization of Earth-bound solar-sail control laws, leveraging (semi-) analytical optimization methods to account for both the SRP and PRP accelerations. Finally, the model would provide a versatile tool also for orbit determination applications, including, but not limited to, the in-orbit estimation of solar-sail acceleration parameters [17].

Building upon the spherical sinusoidal PRP acceleration model by Carzana et al. [16] valid for ideal sails, this technical note presents an extension to this model for optical solar sails that is analytical in nature. To determine the PRP acceleration, the model draws on the same theory of sail–radiation interaction used by McInnes to develop the optical SRP acceleration model [1], although considering a different radiation source: the Earth. First, the model's assumptions and full derivation are discussed. Then, using NASA's ACS3 mission as a baseline, a parametric analysis considering several orbital scenarios is conducted. The analysis aims to compare the newly devised model against other state-of-the-art models. The results highlight the new model's accuracy, which is found to be 4–5 times higher than that of the ideal PRP acceleration model by Carzana et al. [16], and comparable to the accuracy of a high-fidelity numerical model, although requiring a fraction of the run time. Finally, the conclusions of the study and possible future expansions of the work are presented.

II. Dynamical Model

The dynamics of an Earth-orbiting solar sail are described using an Earth-centered reference frame, $\mathcal{I}(x, y, z)$, with the x axis toward the vernal equinox, the z axis perpendicular to the equator and positive toward the North Pole, and the y axis completing the right-handed frame. Within this frame, the solar-sail dynamics can be expressed as

$$\ddot{\boldsymbol{r}} + \frac{\mu}{r^3}\boldsymbol{r} = \boldsymbol{a}_{\mathrm{SRP}} + \boldsymbol{a}_{\mathrm{BBRP}} + \boldsymbol{a}_{\mathrm{ARP}} \tag{1}$$

In Eq. (1), $\mu = 398600.4415\ \mathrm{km^3\,s^{-2}}$ is the Earth's gravitational parameter [26], $\boldsymbol{r} = [x, y, z]^T$ is the sailcraft position vector, $r = \|\boldsymbol{r}\|$, $\boldsymbol{a}_{\mathrm{SRP}}$ represents the SRP acceleration, and $\boldsymbol{a}_{\mathrm{BBRP}}$ and $\boldsymbol{a}_{\mathrm{ARP}}$ denote the two possible types of PRP acceleration, that is, the blackbody radiation pressure (BBRP) and albedo radiation pressure (ARP) accelerations, respectively. The full expressions of these accelerations are provided in the following sections. Note that, in the following, PRP will serve as a unifying term to refer to either BBRP or ARP.

Received 11 November 2024; accepted for publication 21 February 2025; published online 28 March 2025.

*Ph.D. Candidate, Faculty of Aerospace Engineering, Delft University of Technology; L.Carzana@tudelft.nl (Corresponding Author).

†Full Professor, Faculty of Aerospace Engineering, Delft University of Technology; P.N.A.M.Visser@tudelft.nl.

‡Associate Professor, Faculty of Aerospace Engineering, Delft University of Technology; M.J.Heiligers@tudelft.nl.

A. Solar Radiation Pressure Acceleration

The SRP acceleration is defined using the optical sail model devised by McInnes [1], valid for fully opaque (nontransmissive) solar sails. Contrary to the ideal sail model, which assumes the sail to behave as a perfect reflector [1], the optical sail model accounts for the nonideal, optical properties of the sail through its optical coefficients, namely, the absorptivity, specular reflectivity, diffuse reflectivity, and emissivity. The corresponding optical SRP acceleration, $\boldsymbol{a}_{\mathrm{SRP}}$, is found from the sum of its components normal to the sail, $\boldsymbol{a}_{\mathrm{SRP},n}$, and tangential to the sail, $\boldsymbol{a}_{\mathrm{SRP},t}$:

$$\boldsymbol{a}_{\mathrm{SRP}} = \boldsymbol{a}_{\mathrm{SRP},n} + \boldsymbol{a}_{\mathrm{SRP},t} \tag{2}$$

$$\boldsymbol{a}_{\mathrm{SRP},n} = \nu\frac{\mathbb{P}_\oplus}{\sigma}\left[\left(1+\tilde{r}_f s_f\right)\cos^2\alpha + \left(1-s_f\right)\tilde{r}_f B_f\cos\alpha + \left(1-\tilde{r}_f\right)\frac{\varepsilon_f B_f - \varepsilon_b B_b}{\varepsilon_f+\varepsilon_b}\cos\alpha\right]\hat{\boldsymbol{n}} \tag{3}$$

$$\boldsymbol{a}_{\mathrm{SRP},t} = \nu\frac{\mathbb{P}_\oplus}{\sigma}\left(1-\tilde{r}_f s_f\right)\cos\alpha\sin\alpha\,\hat{\boldsymbol{t}} \tag{4}$$

As illustrated in Fig. 1, $\hat{\boldsymbol{n}}$ represents the sail-normal direction with a positive component along the sunlight direction, $\hat{\boldsymbol{s}}$, and $\hat{\boldsymbol{t}}$ is the transversal direction defined as

$$\hat{\boldsymbol{t}} = \hat{\boldsymbol{n}}\times\frac{\left(\hat{\boldsymbol{s}}\times\hat{\boldsymbol{n}}\right)}{\left\|\hat{\boldsymbol{s}}\times\hat{\boldsymbol{n}}\right\|} \tag{5}$$

In Eqs. (3) and (4), σ is the sailcraft mass-to-sail area ratio, and $\nu\in[0,1]$ represents the shadow factor, which accounts for the effect of eclipses. Its value is computed using a conical shadow model similar to the one presented in Refs. [8,27], although considering $\nu=0$ not only in the umbra, but also in the penumbra. This means that no sunlight is assumed to reach the sailcraft when this is in partial eclipse, as the latter is conservatively treated as full eclipse. $\mathbb{P}_\oplus$ is the SRP at 1 AU from the Sun:

$$\mathbb{P}_\oplus = \frac{\mathbb{S}_\oplus}{c} \tag{6}$$

where $\mathbb{S}_\oplus = 1367\ \mathrm{W/m^2}$ is the solar flux at Earth [26] and $c = 299792.458$ km/s is the speed of light in vacuum [28]. The solar-sail pitch angle is indicated by $\alpha\in[0,\pi/2]$ and is measured between $\hat{\boldsymbol{s}}$ and $\hat{\boldsymbol{n}}$; see Fig. 1. Finally, the optical properties of the sail are specified through the reflectivity $\tilde{r}$, specular reflection coefficient s, non-Lambertian reflection coefficient B, and emissivity ε, with the subscript "f" or "b" indicating whether the optical coefficient refers to the front or back of the sail, respectively. Note that Eqs. (3) and (4) are based on the assumption that only the sail's front is exposed to sunlight and the back is never illuminated [1]. As a result, $\hat{\boldsymbol{n}}$ always points out of the back of the sail, see Fig. 1, and the normal and transversal components of the SRP acceleration do not depend on the reflectivity and specular reflection coefficient of the sail backside, $\tilde{r}_b$ and s_b. In real-life solar-sail missions, sunlight may illuminate also the back of the sail. Although an SRP acceleration model that accounts for this possibility exists in the literature [17], the assumption made in this note, that sunlight only reaches the front of the sail, is in line with the analyses conducted in Sec. III. Indeed, in that section, locally optimal steering laws developed under the same assumption will be considered. It should be noted that, unlike for sunlight, these steering laws do not prevent planetary radiation from illuminating the back of the sail. As discussed in the next section, this makes knowledge of $\tilde{r}_b$ and s_b essential to compute the PRP acceleration, as opposed to the SRP acceleration.

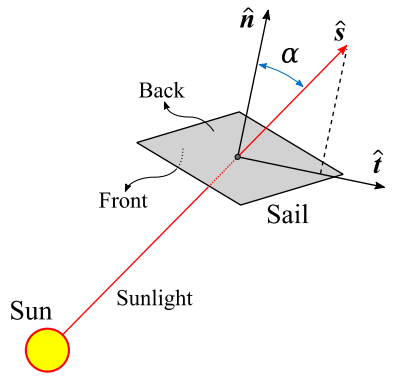

Fig. 1 Geometry of the optical SRP acceleration model.

B. Planetary Radiation Pressure Acceleration

In this section, the PRP acceleration model for optical solar sails is derived. This model forms an extension of the spherical sinusoidal PRP acceleration model presented in Ref. [16], valid for double-sided perfectly reflecting (ideal) solar sails. Although these two PRP acceleration models represent the sail optical properties differently, they also share common characteristics, particularly the assumption that the sail is flat and the way the Earth's planetary radiation distribution is represented. Indeed, in both models the Earth is assumed to be a spherical radiation source emitting blackbody and albedo radiation with varying intensity across its surface. The emitted blackbody radiation flux is assumed to vary sinusoidally with latitude, with a maximum at the equator. On the other hand, the emitted albedo radiation flux is computed while assuming the Earth's albedo coefficient to vary sinusoidally (with maxima at the poles) and accounting for the illumination conditions of the Earth's surface through a so-called phase function. This function is maximum at the subsolar point and decreases moving toward the dark side of the Earth, where it attains a value of zero, indicating the complete absence of albedo radiation. Finally, the planetary radiation flux at the sail's location, S, is determined by assuming that the blackbody and albedo radiation fluxes found are uniformly spread over the visible surface of the Earth as seen from the sailcraft. In this way, the Earth is locally approximated as an isotropic radiation source, allowing the PRP acceleration to be expressed analytically. As discussed in Ref. [16], this approximation introduces an error, but its impact on sailcraft maneuverability is limited, as relative errors compared to a high-fidelity numerical model consistently in the order of 1% are found across several orbital scenarios. For more information on the derivation of the planetary flux, S, the reader is referred to Ref. [16]. Throughout the remainder of this section, the value of S will be assumed to be known.

As defined in Eq. (15) of Ref. [16], the radiation pressure at the sail's location due to the radiation emitted by a differential element of Earth surface, dA, is

$$d\mathbb{P} = \frac{S}{\pi c}\frac{\cos\vartheta}{l^2}\,dA \tag{7}$$

where l is the distance between the surface element dA and the sail, and $\vartheta\in[0,\pi/2]$ is the angle between the normal direction to dA, $\hat{\boldsymbol{N}}$, and the direction from dA to the sail, $\hat{\boldsymbol{l}}$; see Fig. 2. The optical PRP acceleration given by the differential element of radiation pressure $d\mathbb{P}$, $d\boldsymbol{a}_{\mathrm{PRP}}$, can be found by adding the acceleration components normal to the sail, $d\boldsymbol{a}_{\mathrm{PRP},n}$, and tangential to the sail, $d\boldsymbol{a}_{\mathrm{PRP},t}$, similarly to the optical SRP acceleration given in Eqs. (2)–(4):

$$d\boldsymbol{a}_{\mathrm{PRP}} = d\boldsymbol{a}_{\mathrm{PRP},n} + d\boldsymbol{a}_{\mathrm{PRP},t} \tag{8}$$

$$d\boldsymbol{a}_{\mathrm{PRP},n} = \frac{d\mathbb{P}}{\sigma}\left[\left(1+\tilde{r}_{lit}s_{lit}\right)\cos^2\theta\,\hat{\boldsymbol{n}}_l + \left(1-s_{lit}\right)\tilde{r}_{lit}B_{lit}\cos\theta\,\hat{\boldsymbol{n}}_l + \left(1-\tilde{r}_{lit}\right)\frac{\varepsilon_f B_f - \varepsilon_b B_b}{\varepsilon_f+\varepsilon_b}\cos\theta\,\hat{\boldsymbol{n}}\right] \tag{9}$$

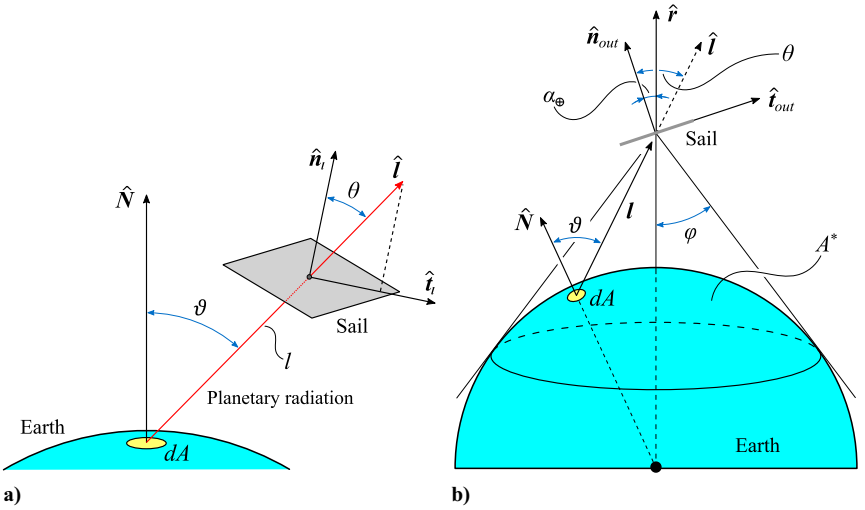

Fig. 2 Geometry to determine the optical PRP acceleration.

$$d\boldsymbol{a}_{\mathrm{PRP},t} = \frac{d\mathbb{P}}{\sigma}\left(1-\tilde{r}_{lit}s_{lit}\right)\cos\theta\sin\theta\,\hat{\boldsymbol{t}}_l \tag{10}$$

It should be noted that Eqs. (9) and (10) share the same structure as Eqs. (3) and (4) for the optical SRP acceleration because they describe the same physical phenomenon, that is, the acceleration produced by radiation when interacting with a sail with given optical properties. This analogy is evidenced also by the sketches of Fig. 1 and Fig. 2a, which depict an equivalent geometry and differ only in the radiation source considered and the side of the sail exposed to the incoming radiation. Indeed, unlike sunlight, the radiation emitted by a surface element dA may also illuminate the back of the sail. An example is shown in Fig. 3, which illustrates how planetary radiation may impinge on either side of the sail, depending on the sail orientation and surface element dA considered. In view of this, the subscript "*lit*" is used in Eqs. (9) and (10) to specify the optical coefficients of the sail side illuminated by the radiation emitted by the surface element dA considered. Equations (9) and (10) also make use of the angle $\theta \in [0, \pi/2]$, which forms the equivalent of the SRP acceleration's pitch angle, α, and is measured between $\hat{\boldsymbol{l}}$ and the sail-normal direction with a positive component along $\hat{\boldsymbol{l}}$, $\hat{\boldsymbol{n}}_l$; see Fig. 2a. Finally, $\hat{\boldsymbol{t}}_l$ represents the transversal direction relative to dA, which can be found from Eq. (5) by substituting $\hat{\boldsymbol{t}}_l$ for $\hat{\boldsymbol{t}}$ and $\hat{\boldsymbol{l}}$ for $\hat{\boldsymbol{s}}$.

Substitution of Eq. (7) in Eqs. (9) and (10) yields

$$\begin{aligned} d\boldsymbol{a}_{\mathrm{PRP},n} = \frac{S}{\pi c\sigma}\Bigg[&\left(1+\tilde{r}_{lit}s_{lit}\right)\frac{\cos\vartheta\cos^2\theta}{l^2}\hat{\boldsymbol{n}}_l \\ &+\left(1-s_{lit}\right)\tilde{r}_{lit}B_{lit}\frac{\cos\vartheta\cos\theta}{l^2}\hat{\boldsymbol{n}}_l \\ &+\left(1-\tilde{r}_{lit}\right)\frac{\varepsilon_f B_f-\varepsilon_b B_b}{\varepsilon_f+\varepsilon_b}\frac{\cos\vartheta\cos\theta}{l^2}\hat{\boldsymbol{n}}\Bigg]dA \end{aligned} \tag{11}$$

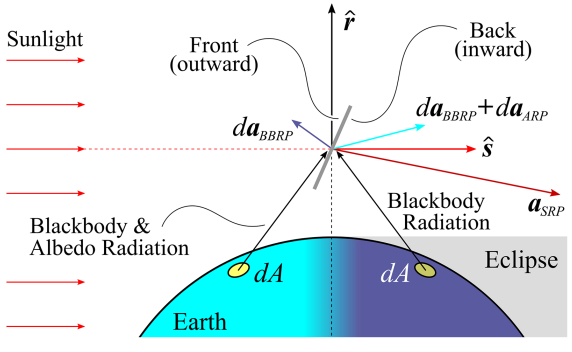

Fig. 3 Sail sides illuminated by sunlight and planetary radiation.

$$d\boldsymbol{a}_{\mathrm{PRP},t} = \frac{S}{\pi c\sigma}\left(1-\tilde{r}_{lit}s_{lit}\right)\frac{\cos\vartheta\cos\theta\sin\theta}{l^2}\hat{\boldsymbol{t}}_l\,dA \tag{12}$$

Using the preceding expressions for $d\boldsymbol{a}_{\mathrm{PRP},n}$ and $d\boldsymbol{a}_{\mathrm{PRP},t}$, Eq. (8) can be integrated over the entire surface of the Earth visible from the sailcraft, A^*; see Fig. 2b. This yields the total PRP acceleration exerted on the solar sail:

$$\boldsymbol{a}_{\mathrm{PRP}} = \int_{A^*} d\boldsymbol{a}_{\mathrm{PRP}} = \int_{A^*}\left(d\boldsymbol{a}_{\mathrm{PRP},n}+d\boldsymbol{a}_{\mathrm{PRP},t}\right) \tag{13}$$

The PRP acceleration integral of Eq. (13) depends on the Earth-sail relative geometry and, most importantly, on the definition of the planetary radiation flux, S. Indeed, depending on how the planetary flux distribution across the surface A^* is modeled, a closed-form solution to the PRP acceleration integral may or may not exist. As mentioned at the beginning of this section, in this study the visible surface A^* is assumed to irradiate isotropically, that is, with a constant radiation flux, S. With this assumption, the integral of Eq. (13) can be solved analytically, yielding the following expression for the optical PRP acceleration:

$$\begin{aligned} \boldsymbol{a}_{\mathrm{PRP}} = \frac{S}{c\sigma}\Bigg\{&\frac{2}{3}\Big[\left(1+\tilde{r}_{in}s_{in}\right)G_{\mathrm{FNS},in}-\left(1+\tilde{r}_{out}s_{out}\right)G_{\mathrm{FNS},out}\Big]\hat{\boldsymbol{n}}_{out} \\ &+\Big[\left(1-s_{in}\right)\tilde{r}_{in}B_{in}G_{\mathrm{FND},in}-\left(1-s_{out}\right)\tilde{r}_{out}B_{out}G_{\mathrm{FND},out}\Big]\hat{\boldsymbol{n}}_{out} \\ &+\frac{\varepsilon_f B_f-\varepsilon_b B_b}{\varepsilon_f+\varepsilon_b}\Big[\left(1-\tilde{r}_{in}\right)G_{\mathrm{FND},in}+\left(1-\tilde{r}_{out}\right)G_{\mathrm{FND},out}\Big]\hat{\boldsymbol{n}} \\ &+\frac{2}{3\pi}\Big[\left(1-\tilde{r}_{in}s_{in}\right)G_{\mathrm{FT},in}+\left(1-\tilde{r}_{out}s_{out}\right)G_{\mathrm{FT},out}\Big]\hat{\boldsymbol{t}}_{out}\Bigg\} \end{aligned} \tag{14}$$

Because planetary radiation can illuminate both sides of the sail simultaneously, the subscripts "*in*" and "*out*" are used to refer to the inward and outward sides of the sail relative to the Earth; see Fig. 3. The outward-pointing sail-normal and transversal directions, $\hat{\boldsymbol{n}}_{out}$ and $\hat{\boldsymbol{t}}_{out}$, respectively, are displayed in Fig. 2b. Recalling that the sail-normal direction $\hat{\boldsymbol{n}}$, defined in Sec. II.A, always points out from the back of the sail, $\hat{\boldsymbol{n}}_{out} = \mathrm{sgn}(\hat{\boldsymbol{n}}\cdot\hat{\boldsymbol{r}})\hat{\boldsymbol{n}}$, whereas $\hat{\boldsymbol{t}}_{out}$ is found from Eq. (5) by substituting $\hat{\boldsymbol{t}}_{out}$ for $\hat{\boldsymbol{t}}$, $\hat{\boldsymbol{n}}_{out}$ for $\hat{\boldsymbol{n}}$, and the radial direction, $\hat{\boldsymbol{r}}$, for $\hat{\boldsymbol{s}}$. Finally, the optical coefficients of the inward, outward, front, and back sides of the sail can be related as follows:

$$\begin{aligned} &\begin{bmatrix}\tilde{r}_{in} & s_{in} & B_{in} & \varepsilon_{in} & \tilde{r}_{out} & s_{out} & B_{out} & \varepsilon_{out}\end{bmatrix} \\ &= \begin{cases}\begin{bmatrix}\tilde{r}_f & s_f & B_f & \varepsilon_f & \tilde{r}_b & s_b & B_b & \varepsilon_b\end{bmatrix} & \text{if } \hat{\boldsymbol{n}}\cdot\hat{\boldsymbol{r}}\geq 0 \\ \begin{bmatrix}\tilde{r}_b & s_b & B_b & \varepsilon_b & \tilde{r}_f & s_f & B_f & \varepsilon_f\end{bmatrix} & \text{otherwise}\end{cases} \end{aligned} \tag{15}$$

It should be noted that, in Eq. (14) and the remainder of this note, $\boldsymbol{a}_{\mathrm{PRP}}$ is used to indicate either the BBRP acceleration, $\boldsymbol{a}_{\mathrm{BBRP}}$, or ARP acceleration, $\boldsymbol{a}_{\mathrm{ARP}}$. For each of these accelerations, a specific radiation flux, S, and set of sail optical coefficients should be considered because the Earth's albedo and blackbody radiations can differ greatly in intensity and, notably, in wavelength. Albedo radiation is emitted in the same wavelength band as solar radiation (0.25–2.8 μm), whereas blackbody radiation is emitted in the infrared band (3–30 μm) [29,30]. Because the sail material responds differently to different wavelengths of the incoming radiation, wavelength-specific sets of optical coefficients should be considered. In the remainder of this note, the following sets of optical coefficients for the albedo and blackbody radiation, $\boldsymbol{oc}_{\mathrm{ARP}}$ and $\boldsymbol{oc}_{\mathrm{BBRP}}$, respectively, will be used:

$$\begin{aligned}\boldsymbol{oc}_{\mathrm{ARP}} &= \begin{bmatrix}\tilde{r}_f & s_f & B_f & \varepsilon_f & \tilde{r}_b & s_b & B_b & \varepsilon_b\end{bmatrix}\\ &= \begin{bmatrix}0.90 & 0.82 & 0.79 & 0.03 & 0.43 & 0.53 & 2/3 & 0.60\end{bmatrix}\end{aligned} \tag{16}$$

$$\begin{aligned}\boldsymbol{oc}_{\mathrm{BBRP}} &= \begin{bmatrix}\tilde{r}_f & s_f & B_f & \varepsilon_f & \tilde{r}_b & s_b & B_b & \varepsilon_b\end{bmatrix}\\ &= \begin{bmatrix}0.97 & 0.82 & 0.79 & 0.03 & 0.40 & 0.53 & 2/3 & 0.60\end{bmatrix}\end{aligned} \tag{17}$$

These optical coefficients refer to NASA's ACS3 solar sail,[§] whose membrane is nontransmissive and consists of a polymer film (polyethelene nepthalate) with an aluminum coating on the front and chromium on the back [29].

In Eq. (14), G_{FNS}, G_{FND}, and G_{FT} indicate the so-called normal specular, normal diffuse, and transversal geometrical factors, respectively. As their names suggest, the geometrical factors express the dependency of the optical PRP acceleration on the Earth-sail geometrical configuration and, similar to the optical coefficients, are specified for both the inward-facing and outward-facing sides of the sail. Denoting A^*_{in} and A^*_{out} as the regions of the surface A^* that are visible from the inward and outward sides of the sail, respectively, the geometrical factors can be defined as

$$G_{\mathrm{FNS},} = \frac{3}{2\pi}\int_{A^*}\frac{\cos\vartheta\cos^2\theta}{l^2}\,dA \tag{18}$$

$$G_{\mathrm{FND},\Diamond} = \frac{1}{\pi}\int_{A^*_{\Diamond}}\frac{\cos\vartheta\cos\theta}{l^2}\,dA \tag{19}$$

$$G_{\mathrm{FT},\Diamond} = \frac{3}{2}\int_{A^*_{\Diamond}}\frac{\cos\vartheta\cos\theta\sin\theta}{l^2}\,dA \tag{20}$$

where "$\Diamond$" is used as a placeholder to indicate either "*in*" or "*out*." The full analytical solutions to the surface integrals on the right-hand side of Eqs. (18)–(20) are provided in the following subsections. As will be shown, these solutions depend only on the orbital radius, r, the planetary pitch angle, $\alpha_\oplus \in [0, \pi/2]$, measured between $\hat{\boldsymbol{n}}_{out}$ and $\hat{\boldsymbol{r}}$, and the maximum view angle between $-\hat{\boldsymbol{r}}$ and the direction from the sailcraft to the Earth's tangent, $\varphi \in (0, \pi/2)$; see Fig. 2b.

1. Normal Specular Geometrical Factor

Depending on the sail orientation with respect to the Earth, two possible configurations can be identified:

a) If $\alpha_\oplus + \varphi \le \pi/2$, the incoming radiation from the visible surface A^* illuminates only the inward side of the sail. In this case, the outward geometrical factor is $G_{\mathrm{FNS},out} = 0$, whereas the inward geometrical factor, $G_{\mathrm{FNS},in}$, is

$$G_{\mathrm{FNS},in} = 1 - \sqrt{1-H^2}\left[1 - H^2\left(1 - \frac{3}{2}\sin^2\alpha_\oplus\right)\right] \tag{21}$$

where the adimensional inverse orbital radius, $H = R/r$, was introduced for conciseness, with $R = 6378.1363$ km the Earth radius [26].

b) If $\alpha_\oplus + \varphi > \pi/2$, both the inward and outward sides of the sail are illuminated; see Fig. 2b and Fig. 3. The corresponding geometrical factors are

$$\begin{aligned}G_{\mathrm{FNS},in} = 1 - \frac{1}{\pi}\Bigg\{&\frac{1}{2}\sqrt{1-H^2}\left[H^2\left(1-3\cos^2\alpha_\oplus\right)+2\right]\cos^{-1}(-A)\\ &+\tan^{-1}B - \frac{3}{2}B^3\cos^4\alpha_\oplus - \frac{1}{2}B\cos^2\alpha_\oplus\left(3\cos^2\alpha_\oplus - 1\right)\Bigg\}\end{aligned} \tag{22}$$

$$\begin{aligned}G_{\mathrm{FNS},out} = \frac{1}{\pi}\Bigg\{&-\frac{1}{2}\sqrt{1-H^2}\left[H^2\left(1-3\cos^2\alpha_\oplus\right)+2\right]\cos^{-1}A\\ &+\tan^{-1}B - \frac{3}{2}B^3\cos^4\alpha_\oplus - \frac{1}{2}B\cos^2\alpha_\oplus\left(3\cos^2\alpha_\oplus - 1\right)\Bigg\}\end{aligned} \tag{23}$$

where the following coefficients are used for conciseness:

$$A = \frac{\cos\alpha_\oplus}{\sin\alpha_\oplus}\sqrt{\frac{1}{H^2}-1}; \quad B = \sqrt{\frac{H^2}{\cos^2\alpha_\oplus}-1} \tag{24}$$

2. Normal Diffuse Geometrical Factor

The normal diffuse geometrical factors correspond to the view factors of the sail sides with respect to the Earth. Their expressions were found by F.G. Cunningham in Ref. [31] and are reported here for completeness:

a) If $\alpha_\oplus + \varphi \le \pi/2$, $G_{\mathrm{FND},out} = 0$ and $G_{\mathrm{FND},in}$ is

$$G_{\mathrm{FND},in} = H^2\cos\alpha_\oplus \tag{25}$$

b) If $\alpha_\oplus + \varphi > \pi/2$, $G_{\mathrm{FND},in}$ and $G_{\mathrm{FND},out}$ are

$$\begin{aligned}G_{\mathrm{FND},in} = \frac{1}{2} - \frac{1}{\pi}\Bigg\{&\sin^{-1}\left(\frac{H}{\sin\alpha_\oplus}\sqrt{\frac{1}{H^2}-1}\right)\\ &+ B\cos\alpha_\oplus\sqrt{1-H^2} - H^2\cos\alpha_\oplus\cos^{-1}(-A)\Bigg\}\end{aligned} \tag{26}$$

$$\begin{aligned}G_{\mathrm{FND},out} = \frac{1}{2} - \frac{1}{\pi}\Bigg\{&\sin^{-1}\left(\frac{H}{\sin\alpha_\oplus}\sqrt{\frac{1}{H^2}-1}\right)\\ &+ B\cos\alpha_\oplus\sqrt{1-H^2} + H^2\cos\alpha_\oplus\cos^{-1}A\Bigg\}\end{aligned} \tag{27}$$

3. Transversal Geometrical Factor

Similar to the other geometrical factors, the definition of the transversal geometrical factor depends on whether only a single or both sides of the sail are illuminated:

a) If $\alpha_\oplus + \varphi \le \pi/2$, $G_{\mathrm{FT},out} = 0$, and $G_{\mathrm{FT},in}$ is

$$G_{\mathrm{FT},in} = \frac{3\pi}{4}H^2\sqrt{1-H^2}\sin(2\alpha_\oplus) \tag{28}$$

b) If $\alpha_\oplus + \varphi > \pi/2$, $G_{\mathrm{FT},in}$ and $G_{\mathrm{FT},out}$ are

$$\begin{aligned}G_{\mathrm{FT},in} = \frac{1}{2}\Bigg\{&B\left[2\sin\alpha_\oplus\cos^3\alpha_\oplus\left(B^2+2+\frac{\cos^2\alpha_\oplus}{\sin^2\alpha_\oplus}\right)\right.\\ &\left.-(1+H^2)\frac{\cos^3\alpha_\oplus}{\sin\alpha_\oplus}\right] + 3H^2\sqrt{1-H^2}\sin\alpha_\oplus\cos\alpha_\oplus\cos^{-1}(-A)\Bigg\}\end{aligned} \tag{29}$$

[§]ACS3 optical coefficients taken from personal communication with J. Ho Kang, Advanced Materials and Processing Branch, NASA Langley Research Center, March 2024.

Table 1 PRP acceleration models considered in Sec. III

Models			Optical coefficients	
PRP acceleration	Planetary flux	Solar sail	$\boldsymbol{oc}_{\text{ARP}}$	$\boldsymbol{oc}_{\text{BBRP}}$
NRTDM	Based on numerical maps	Optical	[0.90 0.82 0.79 0.03 0.43 0.53 2/3 0.60]	[0.97 0.82 0.79 0.03 0.40 0.53 2/3 0.60]
Optical sinusoidal	Sinusoidal dependence on latitude	Optical	[0.90 0.82 0.79 0.03 0.43 0.53 2/3 0.60]	[0.97 0.82 0.79 0.03 0.40 0.53 2/3 0.60]
Ideal sinusoidal	Sinusoidal dependence on latitude	Ideal	[1 1 2/3 0 1 1 2/3 0]	[1 1 2/3 0 1 1 2/3 0]
No PRP	(absent)	N/A	N/A	N/A

$$G_{\text{FT},out} = \frac{1}{2}\left\{B\sin\alpha_{\oplus}\cos^3\alpha_{\oplus}\left[B^2\left(2-\frac{\cos^2\alpha_{\oplus}}{\sin^2\alpha_{\oplus}}\right)+3\right] - 3H^2\sqrt{1-H^2}\sin\alpha_{\oplus}\cos\alpha_{\oplus}\cos^{-1}A\right\} \tag{30}$$

III. Comparison with State of the Art

In this section, different parametric analyses are presented, which aim to quantify the accuracy of the optical PRP acceleration model compared to other analytical models and a high-fidelity numerical model. To this end, several simulations are performed, considering different initial orbital altitudes, orbit orientations, simulation start times, and PRP acceleration models. The analysis settings, accuracy metric, and results are discussed in the following subsections.

A. Sailcraft Dynamics and Control

For each simulation in the parametric analyses, the dynamics presented in Sec. II are propagated using the following models for the PRP acceleration, $\boldsymbol{a}_{\text{PRP}}$:

1) *Optical NRTDM model.* In this model, the planetary radiation flux is computed numerically from discrete maps of the Earth's albedo coefficient and blackbody radiation flux obtained from the ANGARA software package [20]. This approach allows one to compute the optical PRP acceleration integral of Eq. (13) as a finite sum. Although it is computationally expensive, this method enables a high accuracy and is therefore considered the ground truth against which the other PRP acceleration models will be compared. This algorithm is implemented in the software tool NRTDM (Near Real-Time Density Model) developed at Delft University of Technology [21,32]. Finally, note that this model is employed considering the blackbody and albedo optical coefficients of ACS3 given in Eqs. (16) and (17).

2) *Optical sinusoidal PRP acceleration model* presented in Sec. II.B. The PRP acceleration is found through Eq. (14), with the planetary flux, S, determined analytically as per Ref. [16] for the spherical sinusoidal PRP acceleration model. Similar to the optical NRTDM model, the optical sinusoidal model also considers ACS3's blackbody and albedo optical coefficients; see Eqs. (16) and (17).

3) *Ideal sinusoidal PRP acceleration model.* This model corresponds to the spherical sinusoidal PRP acceleration model developed in Ref. [16] for ideal sails. Note that this model can be found from the optical sinusoidal model using the following set of ideal optical coefficients [1]:

$$\boldsymbol{oc}_{\text{ARP}} = \boldsymbol{oc}_{\text{BBRP}} = \begin{bmatrix}\tilde{r}_f & s_f & B_f & \varepsilon_f & \tilde{r}_b & s_b & B_b & \varepsilon_b\end{bmatrix} = [1 \quad 1 \quad 2/3 \quad 0 \quad 1 \quad 1 \quad 2/3 \quad 0] \tag{31}$$

4) *No-PRP model.* In this model the PRP acceleration is neglected, that is, $\boldsymbol{a}_{\text{PRP}} = \boldsymbol{0}$ at any time.

Note that, for the reader's convenience, the characteristics of the preceding models are summarized in Table 1. The SRP acceleration, $\boldsymbol{a}_{\text{SRP}}$, is computed using the optical model presented in Sec. II.A. Because the albedo and solar radiations are emitted within the same wavelength band, the optical coefficients of Eq. (16) are also used for the SRP acceleration. For each simulation, the solar-sail dynamics are propagated for 10 days, using Matlab's® *ode45* integrator with absolute and relative tolerances of 10^{-12}, while implementing locally optimal orbit-raising and inclination-changing steering laws. These steering laws are computed based on an algorithm similar to the one devised by McInnes for ideal sails [1], although adapted to the optical sail model presented in Sec. II.A. It should be noted that because these steering laws account only for SRP in the optimization process, in the analyses, the PRP acceleration is considered as an uncontrolled perturbing acceleration affecting the orbit.

B. Reference Mission Scenario

The ACS3 mission is used as a baseline scenario in all analyses, with a solar-sail characteristic acceleration of 0.045 mm/s^2 (corresponding to $\sigma = 0.2027$ kg/m^2) and the following vector of initial orbital elements defined in frame $\mathcal{I}(x, y, z)$:

$$\left[a_0, e_0, i_0, \text{LTAN}_0, \omega_0, f_0\right]^T = \left[7093.1363\text{ km}, 0, 98.2490\text{ deg}, \begin{Bmatrix}00{:}00\text{ AM}\\00{:}30\text{ AM}\\\vdots\\11{:}30\text{ PM}\end{Bmatrix}, 0\text{ deg}, 0\text{ deg}\right]^T \tag{32}$$

where a is the semimajor axis, e the eccentricity, i the inclination, ω the argument of perigee, f the true anomaly, LTAN stands for Local Time of the Ascending Node, and the subscript "0" denotes the initial value of these variables.[¶] These orbital elements represent a circular, Sun-synchronous orbit with initial altitude $h_0 = a_0 - R = 715$ km, where the Earth radius, R, is given in Sec. II.B.1. Although this altitude does not coincide with the actual altitude of ACS3 at launch [33], it was chosen for consistency (and to facilitate comparison) with the analyses in Sec. V.B of Ref. [16]. Indeed, these also examine the accuracy of different PRP acceleration models considering the initial orbital elements in Eq. (32), although using *ideal* orbit-raising and inclination-changing steering laws. In Eq. (32), several values of the LTAN are considered, spaced by 0.5 hrs along the entire 24-hour time span. This parameter provides a measure of the relative orientation of the orbital plane with respect to the sunlight direction and it is correlated to the right ascension of the ascending node. Indeed, for an LTAN at 0000 hrs, the right ascension of the ascending node is uniquely determined by the position of the Sun, and each 0.5 hrs increment in LTAN corresponds to a 7.5-degree increment in the right ascension of the ascending node. Finally, the parametric analyses also consider 12 different simulation start times, corresponding to the 15th day of each month of 2024.

C. Accuracy Metric

To compare the accuracy of the four PRP acceleration models presented in Sec. III.A, four propagations are performed for each combination of initial orbit, simulation start time, and steering law. Then, the relative errors between the final altitude/inclination

[¶]ACS3 mission data taken from personal communication with W.K. Wilkie, Principal Investigator of the ACS3 mission, NASA Langley Research Center, February 2024.

obtained by the optical NRTDM model (as mentioned earlier, considered the ground truth) and each one of the other models, ε_{rel}, are computed. The relative error ε_{rel} is defined as

$$\varepsilon_{\text{rel}} = \frac{\left|\text{œ}_{\text{ref},f} - \text{œ}_f\right|}{\text{œ}_{\text{ref},f} - \text{œ}_0} \tag{33}$$

where œ_0 indicates the initial value of the steering law's target parameter (i.e., h or i), and $\text{œ}_{\text{ref},f}$ and œ_f represent the final values of the target parameter found through the optical NRTDM (reference) model and the other models under consideration, respectively.

D. Dependence of Accuracy on LTAN

Figure 4a shows the variation of the relative error with the LTAN for the orbit-raising steering law, for the no-PRP, ideal sinusoidal, and optical sinusoidal acceleration models. For each model, a band is displayed that represents the range of relative errors obtained by considering the 12 simulation start times at each month of 2024. The plot illustrates that all error bands follow a 12-hour periodic trend, approximately symmetric with respect to the LTAN at 1200 hrs. This symmetry is due to the similar relative orientation of the orbital plane to the sunlight direction in Sun-synchronous orbits with a 12 hrs LTAN difference, which therefore yields similar orbit-raising performances. The results show that the error of the optical sinusoidal model is only weakly dependent on the LTAN. On the other hand, the error bands of the no-PRP and ideal sinusoidal models exhibit a more pronounced trend, with larger errors found for LTANs around 0000/1200 hrs. This is because, for these LTANs, the sailcraft flies in the vicinity of the subsolar point once per orbital period, where albedo radiation is most intense. Therefore, the dynamics are more easily perturbed and errors resulting from mismodeling the ARP acceleration are amplified. Conversely, for an LTAN at 0600/1800 hrs, the sailcraft remains close to the day–night terminator throughout its orbit, thus resulting in a minor albedo radiation intensity and smaller errors. It is also interesting to note that the error band of the optical sinusoidal model appears narrower than those of the no-PRP and ideal sinusoidal models. As the width of the error band represents the range of errors achieved when changing the simulation start date, this result highlights the superior accuracy of the optical sinusoidal model also with respect to the simulation start date. The plot shows that neglecting the PRP can induce errors in the altitude gain of up to 12.2%, in agreement with the results found in Ref. [16] for ideal solar-sail steering laws. Accounting for the PRP through the ideal or optical sinusoidal models strongly reduces the error to a maximum of 4.54% and 1.07%, respectively. Note that these models consider the same planetary radiation distribution and only differ in the assumed optical properties of the sail. The difference between the error bands of these two models therefore provides a direct measure of the error introduced when assuming the sail to be a perfect reflector for planetary radiation. Using the optical sinusoidal model yields minor relative errors oscillating between 0.24% and 1.07%. Similar to the results presented in Ref. [16] for the ideal sinusoidal model, this error originates from the approximation that the visible surface of the Earth irradiates isotropically, which can represent a source of error particularly for the ARP acceleration, when the day–night terminator is visible from the sailcraft.

Similar to Fig. 4a, Fig. 4b displays the variation of ε_{rel} for the inclination-changing steering law, for different LTAN values and PRP acceleration models. A 12-hour periodicity in the errors is again obtained, although the error bands appear skewed and asymmetric. This asymmetry is due to the complex nature of the inclination-changing steering law, for which orbits with similar orientations with respect to the sunlight direction still yield different increases in inclination. Similar to the orbit-raising case, small errors are achieved for LTANs around 0600/1800 hrs, due to the minor perturbing effect of the ARP acceleration on the dynamics. Also, the error band of the optical sinusoidal model exhibits a narrower spread compared to the other models, reflecting its lower error variation with the simulation start date. Neglecting the PRP in the dynamics yields large relative errors, even up to 47.5%. The errors of the ideal and optical sinusoidal models, on the other hand, induce smaller errors up to 14.9% and 2.35%, respectively.

E. Dependence of Accuracy on Altitude and Inclination

To assess the accuracy of the optical sinusoidal model at different altitudes and inclinations, the parametric analysis presented in Sec. III.D is repeated first for initial altitudes $h_0 = \{450, 550, 650, 715, 800, 900, 1000\}$ km and their corresponding Sun-synchronous

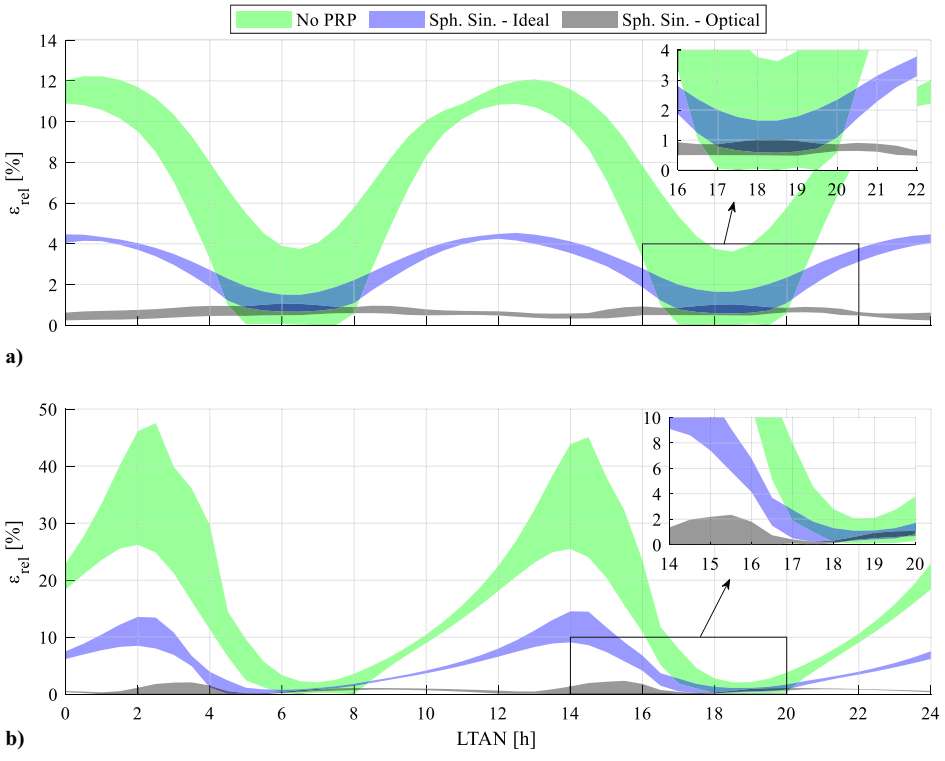

Fig. 4 Relative error on the a) altitude, and b) inclination increase of different PRP acceleration models.

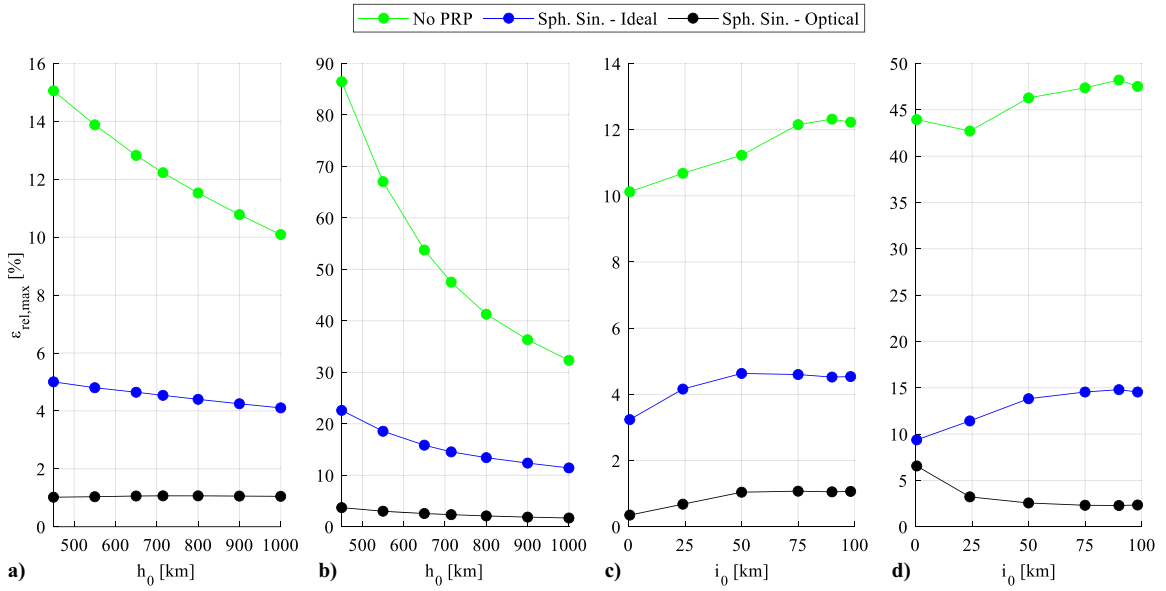

Fig. 5 Maximum relative error on a, c) the altitude increase, and b, d) inclination increase, for different initial altitudes and inclinations.

inclinations, and second, assuming $h_0 = 715$ km and $i_0 = \{0.5, 24, 50, 75, 90, 98.2490\}$ deg, where the last value corresponds to the Sun-synchronous inclination at $h_0 = 715$ km. The results appear in Fig. 5, which displays the maximum relative error achieved over all LTANs and simulation start times, $\epsilon_{\text{rel,max}}$, for each PRP acceleration model, steering law, initial altitude, and inclination. Notably, the optical sinusoidal model performs consistently better than the other models for all cases analyzed. When changing the initial altitude, it achieves values for $\epsilon_{\text{rel,max}}$ of at most 1.07% and 3.7% for the orbit-raising and inclination-changing steering laws, respectively, regardless of the initial altitude; see Figs. 5a and 5b. Similarly, when varying the initial inclination, values for $\epsilon_{\text{rel,max}}$ of 0.35–1.07% and 2.29–6.55% are found for the orbit-raising and inclination-changing steering laws, respectively; see Figs. 5c and 5d. In comparison, the ideal sinusoidal model achieves larger errors, attaining values within 3.23% and 5.00% for the orbit-raising steering law; see Figs. 5a and 5c; and within 9.37% and 22.7% for the inclination-changing steering law; see Figs. 5b and 5d. Finally, neglecting the PRP induces even larger errors, consistently above 10% for all orbit-raising cases analyzed; see again Figs. 5a and 5c; and within 30% and 90% for all the inclination-changing cases analyzed; see Figs. 5b and 5d.

The aforementioned results highlight that, despite its analytical nature, the optical sinusoidal model achieves a very high fidelity for a wide variety of orbital scenarios, even compared to its numerical counterpart. Finally, it is worth noting that the optical model reduces the computational effort compared to the numerical model by a factor of 31. Because both these models are implemented in MATLAB® R2020b, this value is independent of the computing hardware.

IV. Conclusions

This technical note presented a new analytical model for the planetary radiation pressure (PRP) acceleration of optical solar sails. The model was found to predict the orbit-raising and inclination-changing capabilities of NASA's Advanced Composite Solar Sail System sailcraft with relative errors of at most 1% and 6%, respectively, compared to a high-fidelity numerical model. This accuracy marks a significant improvement with respect to the preexistent ideal PRP acceleration model, for which errors up to 5% and 23% were found. The new model furthermore reduces the computational effort compared to its numerical counterpart by a factor of 31. These results therefore demonstrate the effectiveness of the newly devised optical PRP acceleration model for accurately describing the PRP-perturbed solar-sail dynamics.

The proposed optical PRP acceleration model may be used in the design of solar-sail steering laws that leverage PRP to enhance the sailcraft maneuverability. This in turn opens up avenues of research in the PRP-based trajectory optimization of Earth-orbiting sailcraft. Because the proposed model assumes the sail to be nontransmissive, future work may also focus on further extending the model to transmissive or refractive materials. In this way, the model could be applied to a broader range of solar-sail designs, widening its scope of applicability. Finally, although developed for solar sails, it should be noted that the optical PRP acceleration model is applicable to any flat surface illuminated by planetary radiation. Therefore, the model can also be used to compute the PRP acceleration of spacecraft with arbitrarily complex shape, when the latter is represented as a set of adjacent flat surfaces and only the faces exposed to planetary radiation are considered.

Acknowledgments

The authors thank W. Keats Wilkie and Jin Ho Kang from NASA Langley Research Center for sharing the ACS3 solar-sail optical properties and mission data. Also, special thanks go to Christian Siemes and Natalia Hladczuk from Delft University of Technology and Eelco Doornbos from the Koninklijk Nederlands Meteorologisch Instituut (KNMI) for sharing the software tool NRTDM and the ANGARA Earth radiation maps.

References

[1] McInnes, C. R., *Solar Sailing—Technology, Dynamics and Mission Applications*, Springer, Berlin, pp. 19–29, 32–40, 46–51, 136–148. https://doi.org/10.1007/978-1-4471-3992-8

[2] Berthet, M., Schalkwyk, J., Çelik, O., Sengupta, D., Fujino, K., Hein, A. M., Tenorio, L., dos Santos, J. C., Worden, S. P., Mauskopf, P. D., et al., "Space Sails for Achieving Major Space Exploration Goals: Historical Review and Future Outlook," *Progress in Aerospace Sciences*, Vol. 150, Oct. 2024, Paper 101047. https://doi.org/10.1016/j.paerosci.2024.101047

[3] Turyshev, S. G., Garber, D., Friedman, L. D., Hein, A. M., Barnes, N., Batygin, K., Brown, M. E., Cronin, L., Davoyan, A. R., Dubill, A., et al., "Science Opportunities with Solar Sailing Smallsats," *Planetary and Space Science*, Vol. 235, Oct. 2023, Paper 105744. https://doi.org/10.1016/j.pss.2023.105744

[4] Tsuda, Y., Mori, O., and, R. Funase, et al., "Achievement of IKAROS —Japanese Deep Space Solar Sail Demonstration Mission," *Acta Astronautica*, Vol. 82, No. 2, 2013, pp. 183–188. https://doi.org/10.1016/j.actaastro.2012.03.032

[5] Wilkie, W., Fernandez, J., Stohlman, O., Schneider, N., Dean, G., Kang, J., Warren, J., Cook, S., Brown, P., Denkins, T., et al., "An Overview of the NASA Advanced Composite Solar Sail (ACS3)

Technology Demonstration Project," *Proceedings of AIAA Scitech 2021 Forum*, AIAA Paper 2021-1260, 2021. https://doi.org/10.2514/6.2021-1260

[6] Zhao, P., Wu, C., and Li, Y., "Design and Application of Solar Sailing: A Review on Key Technologies," *Chinese Journal of Aeronautics*, Vol. 36, No. 5, 2023, pp. 125–144. https://doi.org/10.1016/j.cja.2022.11.002

[7] Spencer, D. A., Johnson, L., and Long, A. C., "Solar Sailing Technology Challenges," *Aerospace Science and Technology*, Vol. 93, Oct. 2019, Paper 105276. https://doi.org/10.1016/j.ast.2019.07.009

[8] Kelly, P., and Bevilacqua, R., "Geostationary Debris Mitigation Using Minimum Time Solar Sail Trajectories with Eclipse Constraints," *Optimal Control Applications and Methods*, Vol. 42, No. 1, 2021, pp. 279–304. https://doi.org/10.1002/oca.2676

[9] Bianchi, C., Niccolai, L., Mengali, G., and Ceriotti, M., "Preliminary Design of a Space Debris Removal Mission in LEO Using a Solar Sail," *Advances in Space Research*, Vol. 73, No. 8, 2024, pp. 4254–4268. https://doi.org/10.1016/j.asr.2024.01.024

[10] Kim, K., "Preliminary Trajectory Design for Mitigating Debris Utilizing Solar Sailing and Conventional Propulsion," *International Journal of Aeronautical and Space Sciences*, Sept. 2024. https://doi.org/10.1007/s42405-024-00833-2

[11] Carzana, L., Visser, P., and Heiligers, J., "Locally Optimal Control Laws for Earth-Bound Solar Sailing with Atmospheric Drag," *Aerospace Science and Technology*, Vol. 127, Aug. 2022, Paper 107666. https://doi.org/10.1016/j.ast.2022.107666

[12] Stolbunov, V., Ceriotti, M., Colombo, C., and McInnes, C. R., "Optimal Law for Inclination Change in an Atmosphere Through Solar Sailing," *Journal of Guidance, Control, and Dynamics*, Vol. 36, No. 5, 2013, pp. 1310–1323. https://doi.org/10.2514/1.59931

[13] Mengali, G., and Quarta, A. A., "Near-Optimal Solar-Sail Orbit-Raising from Low Earth Orbit," *Journal of Spacecraft and Rockets*, Vol. 42, No. 5, 2005, pp. 954–958. https://doi.org/10.2514/1.14184

[14] De Iuliis, A., Ciampa, F., Felicetti, L., and Ceriotti, M., "Sailing with Solar and Planetary Radiation Pressure," *Advances in Space Research*, Vol. 67, No. 9, 2021, pp. 2795–2811. https://doi.org/10.1016/j.asr.2019.11.036

[15] Barles, A., Ceriotti, M., Ciampa, F., and Felicetti, L., "An Optimal Steering Law for Sailing with Solar and Planetary Radiation Pressure," *Aerospace Science and Technology*, Vol. 118, Nov. 2021, Paper 107051. https://doi.org/10.1016/j.ast.2021.107051

[16] Carzana, L., Visser, P., and Heiligers, J., "A New Model for the Planetary Radiation Pressure Acceleration for Solar Sails," *Journal of Guidance, Control, and Dynamics*, Vol. 47, No. 8, 2023, pp. 1674–1687. https://doi.org/10.2514/1.G007668

[17] Carzana, L., Amodio, A. V. P. Minervino, Wilkie, W. K., and Heiligers, J., "Calibration Steering Laws to Estimate the Optical Properties of NASA's ACS3 Solar Sail," *Proceedings of the 29th International Symposium on Space Flight Dynamics*, European Space Operations Centre (ESOC) and EUMETSAT, April 2024.

[18] Arnold, S. J., and Dow, J. M., "Models for Spacecraft Acceleration due to Earth Albedo and Infrared Radiation," European Space Operations Centre (ESOC) OAD WP 265, Darmstadt, Germany, 1984.

[19] Gini, F., Bardella, M., and Casotto, S., "Precise Non-Gravitational Forces Modeling for GOCE," *Advances in the Astronautical Sciences*, Vol. 152, Jan. 2014, pp. 3141–3157.

[20] Fritsche, B., Ivanov, M., Kashkovsky, A., Koppenwallner, G., Kudryavtsev, A., Voskoboinikov, U., and Zhukova, G., "Radiation Pressure Forces on Complex Spacecraft—Final Report," European Space Operations Centre (ESOC) CR 11908, 1998.

[21] Doornbos, E., Bruinsma, S., Fritsche, B., Koppenwallner, G., Visser, P., Van Den IJssel, J., and de Encarnação, J. D. T., "Algorithm Theoretical Basis Document," *GOCE+ Theme 3: Air Density and Wind Retrieval Using GOCE Data*, ESA CR 4000102847/NL/EL, 2014.

[22] Putney, B., Kolenkiewicz, R., Smith, D., Dunn, P., and Torrence, M., "Precision Orbit Determination at the NASA Goddard Space Flight Center," *Advances in Space Research*, Vol. 10, No. 3-4, 1990, pp. 197–203. https://doi.org/10.1016/0273-1177(90)90350-9

[23] McCarthy, J. J., and Martin, T. V., "A Computer Efficient Model of Earth Albedo Satellite Effects," NASA Goddard Space Flight Center, Planetary Sciences Department Rept. 012-77, 1977.

[24] Betts, J. T., "Survey of Numerical Methods for Trajectory Optimization," *Journal of Guidance, Control, and Dynamics*, Vol. 21, No. 2, 1998, pp. 193–207. https://doi.org/10.2514/2.4231

[25] Montenbruck, O., and Gill, E., Satellite Orbits: Models, Methods and Applications, Springer, Berlin, 2000, pp. 233–291.

[26] Wertz, J. R., and Larson, W. J., *Space Mission Analysis and Design*, Springer, Dordrecht, 2005, pp. 897–898.

[27] Ortiz Longo, C. R., and Rickman, S. L., *Method for the Calculation of Spacecraft Umbra and Penumbra Shadow Terminator Points*, NASA Center for AeroSpace Information, Linthicum Heights, 1995.

[28] Tiesinga, E., Mohr, P. J., Newell, D. B., and Taylor, B. N., "CODATA Recommended Values of the Fundamental Physical Constants: 2018," *Reviews of Modern Physics*, Vol. 93, No. 2, 2021, p. 3. https://doi.org/10.1103/RevModPhys.93.025010

[29] Kang, J. Ho, Gordon, K. L., Bryant, R. G., Stohlman, O. R., Wilkie, W. K., Stark, A. E., Barfield, R. S., Sindle, B. R., Finckenor, M. M., and Craven, P. D., "Durability Characterization of Mechanical Interfaces in Solar Sail Membrane Structures," *Advances in Space Research*, Vol. 67, No. 9, 2021, pp. 2643–2654. https://doi.org/10.1016/j.asr.2020.08.015

[30] Lissauer, J., and de Pater, I., Fundamental Planetary Science: Physics, Chemistry and Habitability, Cambridge Univ. Press, Cambridge, England, U.K., 2013, pp. 86–91, 97–100. https://doi.org/10.1017/9781108304061

[31] Cunningham, F. G., *Power Input to a Small Flat Plate from a Diffusely Radiating Sphere, with Application to Earth Satellites*, National Aeronautics and Space Administration, Washington, D.C., 1961.

[32] Doornbos, E., *Thermospheric Density and Wind Determination from Satellite Dynamics*, Springer, Berlin, 2012. https://doi.org/10.1007/978-3-642-25129-0

[33] Dono, A., Hendriks, T., and Wilkie, W. K., "Navigation for the ACS3 Solar Sail Mission," *Proceedings of the 4S Symposium*, European Space Agency (ESA) and Centre National d'Études Spatiales (CNES), May 2024.

M. Macdonald
Associate Editor